CrossMark

Optimized synthesis and characterization of lutetium carbonate and oxide nanoparticles and their use as degradation photocatalyst

Mehdi Rahimi-Nasrabadi[1] (ORCID) · **Seied Mahdi Pourmortazavi[2]** · **Mohmmad Reza Ganjali[3,4]** · **Parviz Norouzi[3,4]**

Abstract Taguchi robust design (TRD) was used to optimize the process for fabrication lutetium carbonate which was then used for the synthesis of lutetium oxide nano-particles, which were subjected to characterization analyses. Through TRD the significance of variables including the concentrations of lutetium and carbonate ion solutions, and the flow rate at which one reagent was added to the other (Fy), and the reactor temperature during the formation of the carbonate particles in the chemical precipitation stage were evaluated. The optimum conditions were found to lead to the formation of carbonate nano-particles with average diameter of 35 nm, which were then thermally treated at 750 °C in an air atmosphere, to form spherical lutetium oxide (Lu_2O_3) nanoparticles of about 36 nm in average diameter. The produced nanoparticles were studied through SEM, TEM, XRD and FT-IR to evaluate their characteristics, and they were also evaluated as photocatalysts in the UV-induced degradation of methyl orange (MO) in an aqueous media.

✉ Seied Mahdi Pourmortazavi
pourmortazavi@yahoo.com

Mehdi Rahimi-Nasrabadi
rahiminasrabadi@gmail.com; kpmrahimi@ihu.ac.ir

[1] Faculty of Pharmacy, Baqiyatallah University of Medical Sciences, Tehran, Iran

[2] Faculty of Material and Manufacturing Technologies, Malek Ashtar University of Technology, Tehran, Iran

[3] Center of Excellence in Electrochemistry, University of Tehran, Tehran, Iran

[4] Biosensor Research Centre, Endocrinology & Metabolism Molecular and Cellular Research Institute, Tehran University of Medical Sciences, Tehran, Iran

1 Introduction

Many researchers have reported the synthesis inorganic micro/nanomaterials with controlled structures, which can be attributed to the interesting chemical and physical properties of such materials [1–4]. Such compounds are usually prepared through precipitation reactions at very high and near super-saturation conditions. These reactions are influenced by various parameters including the reaction temperature, reagent concentration and mixing conditions. So the formation and growth of the nuclei greatly depend on the concentration of the reagents and the rate at which they are mixed. There have also been reports on the fine-tuning of the morphology and size of the product particles through adding certain agents with non-stoichiometric influences on the reaction outcome [5–8].

Preparing lanthanide compounds such as lutetium carbonate or oxide have attracted some attention due to their promising performance as phosphors, and catalysts, owing to their interesting electronic, optical, and chemical properties [9–11]. Lu_2O_3 has various considerable properties including high melting point and phase stability, and low thermal expansion. The compound is also known to have a wide band gap of 5.2–5.5 eV [12], has a high-κ dielectric constant of about κ = 11–13 [13, 14]. Lu_2O_3 possesses a unique set of characteristics like considerable mechanical strength, hardness, thermal conductivity and can be easily doped with ions of rare earth elements [15].

Rare earth (RE) sesquioxides like lutetium oxide, are hence promising choices for use as laser hosts to be used in high-power lasers and/or those with ultra-short pulses. Lu_2O_3 is also interesting for use in various activators due to its wide band gap. It has also been reported that doping such RE ions as Nd^{3+}, Lu^{3+}, and Eu^{3+}, compounds like Lu_2O_3 find further potential for use in high-power lasers,

given their high thermal conductivity. The compound can also be used in scintillators owing to its high density [11, 16, 17]. Different Lu_2O_3 samples, with different structural properties, i.e. nanoflakes [18], microflowers [19], nanorods [20], core–shell structures [21] and nanocrystals [22] have been prepared through different methods.

Catalysts used in photo-induced reactions has are very attractive green procedures, which have become very attractive recently. Such catalysts, i.e. photocatalysts convert light energy to chemical energy [23–26], and are also known to be environment friendly tools for various environmental issues [27–31] such as removing pollutants, reducing heavy metals, and removing arsenic and Cr(VI) removal. Upon subjecting samples to UV or Vis light in the presence of photocatalysts, different organic contaminants, e.g. nitro-aromatic explosives [32], diclofenac [33], phenol [34], 4-Chlorophenol [35], NOx [36], organic dye [37] have reportedly been decomposed.

As to precipitation reactions, orthogonal array design (OAD) can be used for optimizing the various factor influencing the properties of the product through performing a limited number of preplanned experiments [38–41]. OAD is a fractional factorial design using an orthogonal array for assigning the major factors in a set of experimental combinations [42]. This economical procedure is commonly used for characterizing complicated processes through fewer steps, yet it required a specific design of experiments, as well as specialized statistics for explaining the results [43]. To perform multilevel OAD, each factor is evaluated at more than two levels; and consequently a major curving in the response surface satisfies the nonlinear character [44, 45]. The results could be evaluated through the analysis of variance (ANOVA) to yield object information confirming the significance of the factors studied [46, 47].

Based on the above-mentioned, the present study was focused on optimizing the parameters influencing the direct precipitation of lutetium carbonate through a statistical experiment design, with the aim of preparing the salt in the form of nanoparticles. The composition and morphology of the product was then evaluated. The particles were then used in a thermal decomposition reaction and the thermal decomposition reaction was also studied through thermal analysis so as to determine the best conditions for preparing the resulting lutetium oxide nanoparticles. Review of the literature on the synthesis of lutetium carbonate micro and nanoparticles, revealed that this has been achieved through a range of few methods, but no report was found on the synthesis of nano-particular lutetium carbonate through a reagent or template-free direct precipitation procedure. The resulting products were eventually evaluated as photo-catalysts in the UV-induced degradation of methyl orange (MO).

2 Experimental

2.1 Lutetium carbonate; optimizing the synthesis procedure

Using analytical-grade lutetium chloride and sodium carbonate (Merck Co.) various Lu^{3+}, and CO_3^{2-} solutions were prepared. The lutetium solutions were the added to the carbonate solutions at different flow rates (Fy) under vigorous stirring at different temperatures. Once the precipitation reaction was complete the product was filtered, repeatedly washed with distilled water, and then with ethanol and finally dried at 70 °C for 3 h.

Using the experimental design approach, variables including the concentrations of Lu^{3+} and CO_3^{2-} solutions, the flow rate of adding the cation solution to that of the anion (Fy) and the temperature of the reactor were studied at three different levels, as summarized in Table 1.

2.2 Synthesis of lutetium oxide

To prepare the lutetium oxide nanoparticles (precursor), optimally prepared lutetium carbonate nanoparticles were

Table 1 Orthogonal array designed for parameter optimization in lutetium carbonate synthesis by direct precipitation reaction

Experiment Number	Lu^{3+} Concentration (M)	CO_3^{2-} Concentration (M)	Lu^{3+} Feed flow rate (ml/min)	Temperature (°C)	Size of lutetium carbonate particles (nm)
1	0.01	0.01	2.5	0	47
2	0.01	0.03	10.0	30	68
3	0.01	0.09	40.0	60	66
4	0.03	0.01	10.0	60	59
5	0.03	0.03	40.0	0	43
6	0.03	0.09	2.5	30	44
7	0.09	0.01	40.0	30	48
8	0.09	0.03	2.5	60	47
9	0.09	0.09	10.0	0	42

subjected to a thermal decomposition reaction in furnace. The reaction was performed under an air atmosphere at 750 °C for 3 h. A typical reaction included loading 0.5 grams of the precursor into an alumina crucible, covering the crucible with aluminum foil to avoid loss of the precursor or the product and once the reaction was over the product was collected and used in the next steps.

2.3 Characterization of the nanoparticles

To assess the morphology of the product samples a Philips XL30 scanning electron microscope (SEM) was used. The samples were loaded on a gold film prepared by an SCD005 BAL-TEC Sputter Coater, for the purpose of analyses. XRD studied were conducted on a Rigaku D/max 2500 V instrument with a graphite monochromator and a Cu target.

The FT-IR spectrophotometer used for the studies was a Bruck Equinox 55 and the KBr pellet technique was used for loading the samples into the instrument. Transmission electron microscopic (TEM) studies were also carried out using a Ziess- EM900 instrument. For the TEM studies the samples were coated on the cupper-carbon coated grid.

The TG-DTA thermal analyses were performed using a Stanton TR-01 thermobalance with a differential thermal analysis attachment (STA 1500). To perform the studies 5.0 mg samples of lutetium carbonate samples and a reference (Pt foil) were placed in the pans of the instrument and the heating was performed at 10 °C/min from 40 to 800 °C, while a flow of nitrogen (the purge gas) was applied at 10 °C/min at 1 bar. The UV–Vis diffuse reflectance spectra (UV–Vis DRS) of the solid samples and the UV–Vis spectrometry of the of the organic species in the water samples were obtained using an Avaspec-2048-TEC Avantes
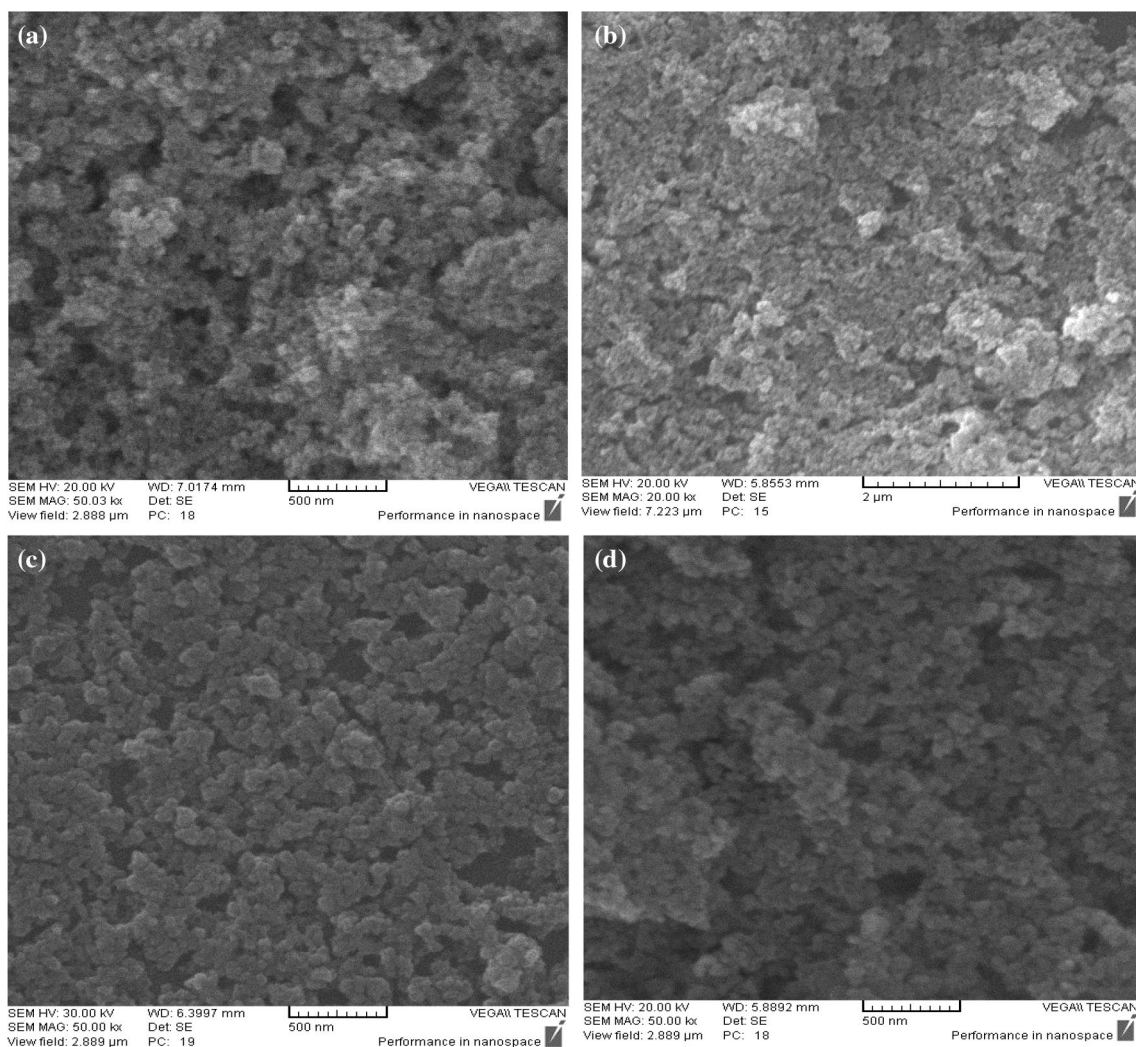

Fig. 1 SEM images of lutetium carbonate nanoparticles obtained under different runs of precipitation reaction (shown in Table 1): **a** run 1, **b** run 4, **c** run 6, and **d** run 8
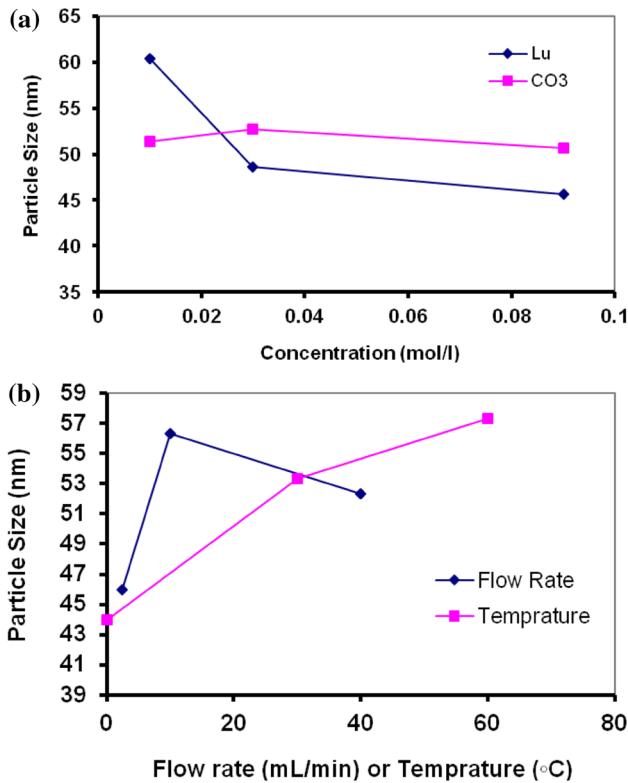
Fig. 2 Main effects for each variable of precipitation reaction on the diameter of the Lutetium carbonate particles

Fig. 3 a SEM image and **b** TEM image of lutetium carbonate nanoparticles prepared via precipitation under optimum conditions

Spectroscope and Spectronix Ar 2015 spectrometer (Electron Engineering Pishro Pajuhesh, Iran). The optical band gap energy (OBGE) of the samples, which shows the energy needed to excite a valence electron to the conduction band in a semiconductor were determined through UV–Vis DRS and Tauc's Eq. [48]:

$$\alpha h\upsilon = A\left(h\upsilon - E_g\right)^{\eta} \tag{1}$$

which shows the relation between the frequency of absorbed light (υ) and OBGE (E_g), using Planck's constant (h), absorption coefficient (α), and constant values (A, η). η was $\frac{1}{2}$ for lutetium carbonate and oxide.

2.4 Evaluation of the photocatalytic activity of the nanoparticles

Lutetium carbonate and oxide nanostructures were added to aqueous solutions of methyl orange (MO) and the suspensions were subjected to UV irradiation in a Pyrex double

Table 2 ANOVA result for synthesis lutetium carbonate nanoparticles using precipitation procedure

Factor[b]	Code	DOF	S	V	Pooled[a]			
					DOF	S´	F´	P´
Lu³⁺ concentration (mol/L)	Lu	2	360.2	180.1	2	360.2	57.9	43.7
Carbonate concentration (mol/L)	CO₃	2	6.2	3.1	–	–	–	–
Flow rate (mL/min)	F	2	162.8	81.4	2	170.7	26.2	19.3
Temperature (°C)	T	2	280.8	140.4	2	270.8	45.1	33.9
Error	E	–	–	–	2	6.2	–	3.1

[a]The critical value was at 90% confidence level; pooled error results from pooling insignificant effect

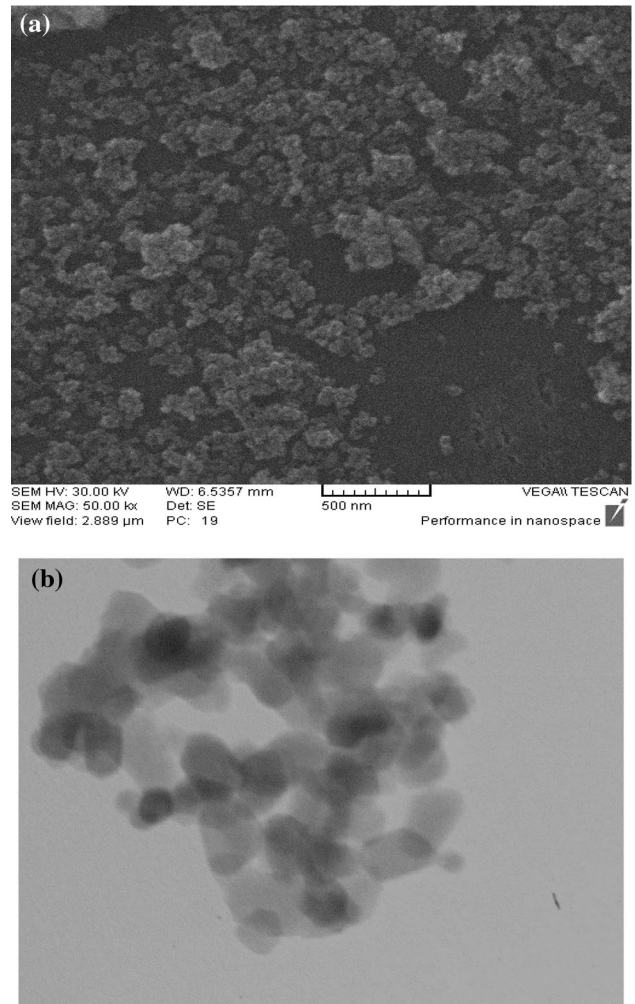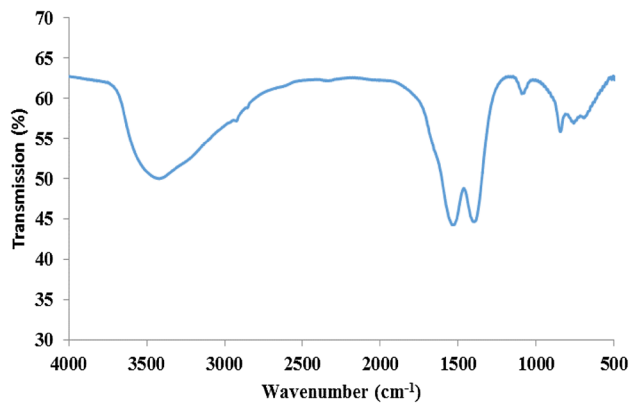[b]Size of synthesized lutetium carbonate particles (nm) were used as response

Fig. 4 FT-IR spectrum of lutetium carbonate nanoparticles prepared with precipitation method

Fig. 6 TG and DTA curves for lutetium carbonate nanoparticles prepared with precipitation method under optimum conditions (sample weight 5.0 mg; heating rate 10 °C/min; nitrogen atmosphere)

pipe air-lift cylinder as a photoreactor. The source of UV light was a high pressure Hg lamp (250 W, $\lambda > 254$ nm) positioned inside the quartz pipe.

The reaction suspension contained 0.1 g/L of each nanoparticle and 5 mg/L of MO and stirred in the dark for 20 min before the reaction. Then the suspensions were subjected to ultraviolet light under aeration and the whole experiment was performed at a constant temperature (25 °C) through cooling the reactor. After the reaction was started at 10 min intervals samples were taken, centrifuged, and studied by UV–Vis spectrometery at the maximum absorption wavelength of MO using the Lambert–Beer law Eq. 2:

$$A = \varepsilon bC \tag{2}$$

A, ε, b and C being absorbance of light, the molar absorptivity, the path length of light through the sample and the concentration of the analyte respectively. Considering C_0 and C as the concentrations of MO in the sample

before the start of the reaction and at each 10 min interval and A_0 and A as the corresponding absorbance values equations 3 and 4 can be obtained from Lambert–Beer law:

$$\frac{A}{A_0} = \frac{C}{C_0} \tag{3}$$

$$\text{Degradation efficiency (\%) } = \frac{A_0 - A_t}{A_0} \times 100 \tag{4}$$

Fig. 7 Diffuse reflectance UV–Vis spectra of as-synthesized, **a** lutetium carbonate (LuCO₃), and **b** lutetium oxide (LuO) nanoparticles
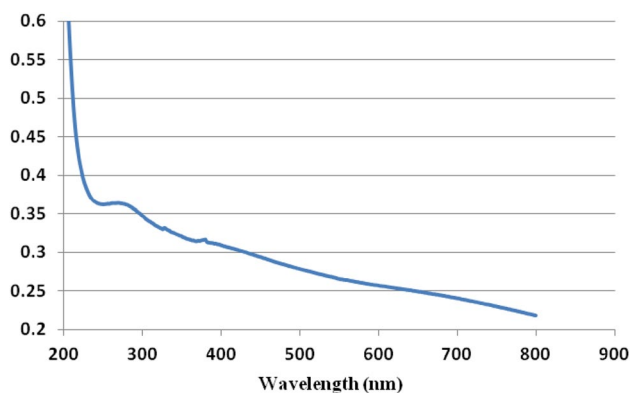

Fig. 5 UV–Vis absorption spectra of the a lutetium carbonate nanoparticles (prepared under optimum conditions of precipitation reaction) dispersed in distilled water
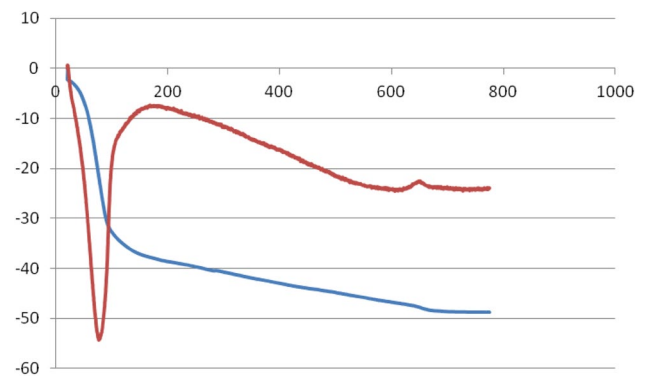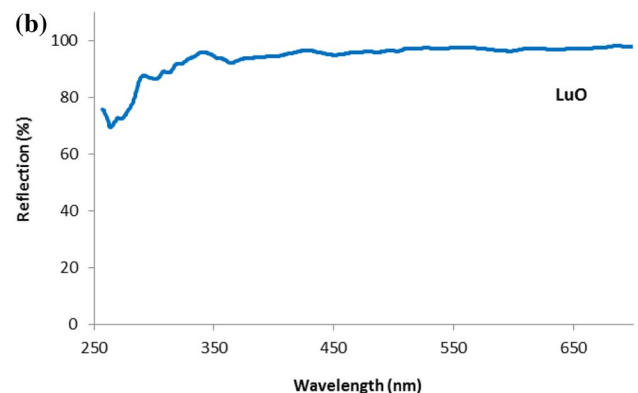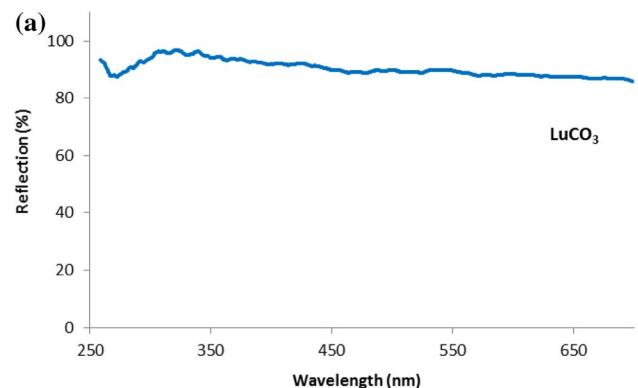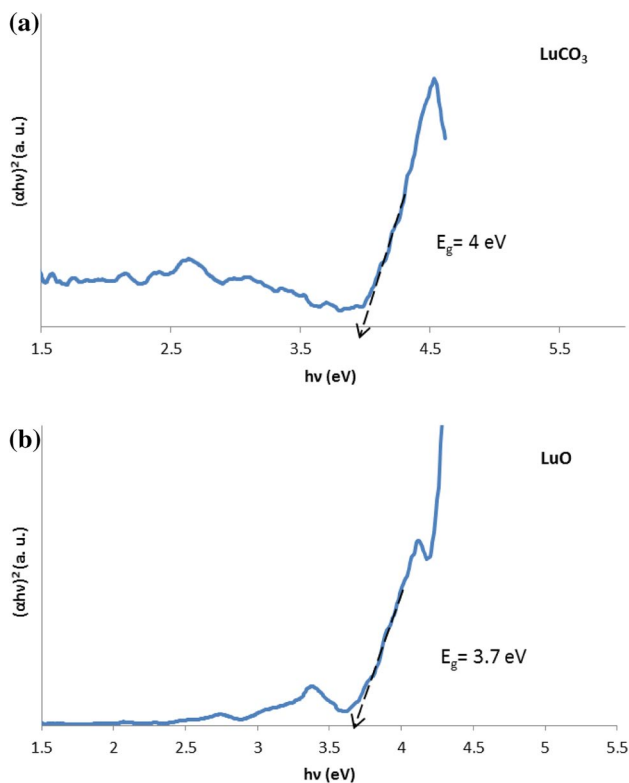
Fig. 8 Tauc's plot for as-prepared, **a** lutetium carbonate (LuCO$_3$), and **b** lutetium oxide (LuO) nanoparticles

The kinetics of the photodegradation reaction was also evaluated against the Langmuir–Hinshelwood kinetics model, which is expressed as:

$$-\frac{dC}{dt} = k_{app}C \tag{5}$$

in which C, k$_{app}$, t and $-\frac{dC}{dt}$ reused for MO concentration, reaction rate constant, degradation time and reaction rate, respectively.

3 Results and discussion

Using direct precipitation reactions (DPR) for preparing insoluble inorganic is a traditionally used procedure [49], while gaining control over the size and morphology of such particles is very complex and requires a detailed understanding of the reaction mechanism. In this light, the present study was focused on using the Taguchi robust design to determine and optimize the overall effect of each reaction parameters on the size and morphology of lutetium carbonate particles prepared through DPR. The factors to be optimized were the concentrations of Lu^{3+} and CO$_3^{2-}$ concentrations, flow rate of the Lu^{3+} when added to the CO$_3^{2-}$ solution (Fy), and the reactor temperature as reported in Table 1.
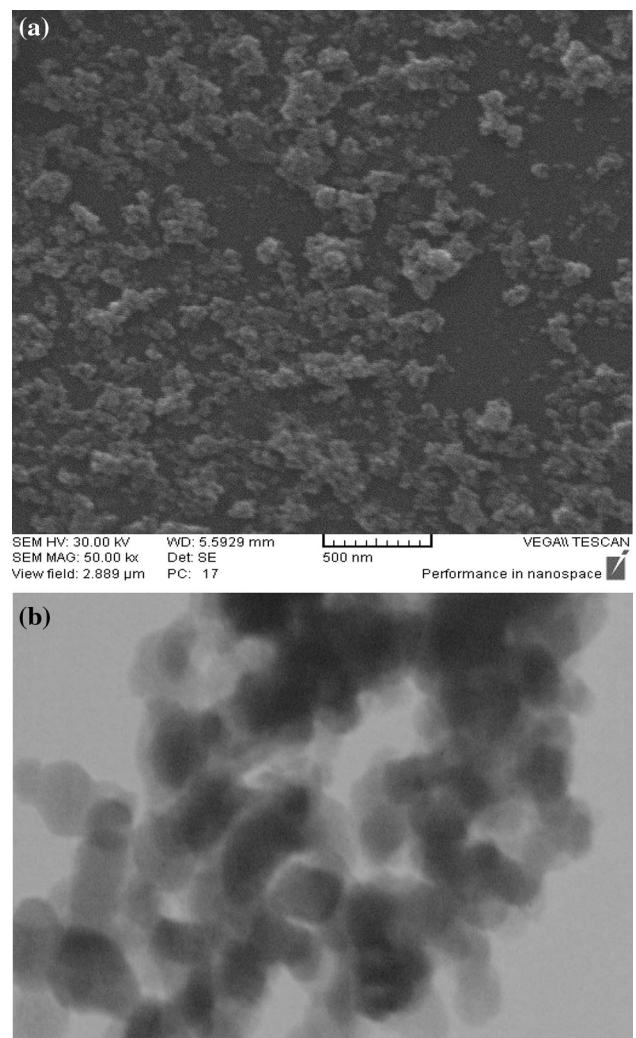

Fig. 9 a SEM and **b** TEM images of lutetium oxide nanoparticles obtained via thermal decomposition of precursor

The SEM images obtained for different lutetium carbonate powder samples obtained through DPR under the conditions of Table 1, are illustrated in Fig. 1. Table 1 also includes the experimental data on the average diameters of the lutetium carbonate particles obtained under each run, which clearly illustrates the relations among the experimental conditions and the properties of the products.

To assess the effects of the different levels of each factor on the properties of the products, the size at each level was determined [48, 49]. In Fig. 2, it can be seen that the mean value of the different levels of each factor indicates the relationship between the particle diameter and the variation of the factors. According to Fig. 2a, changing the concentration of the Lu^{3+} solution at the three different levels of 0.01, 0.03, and 0.09 M leads to considerable changes in the diameter of the product particles, while similar changes in the concentration of carbonate ion solutions at the same

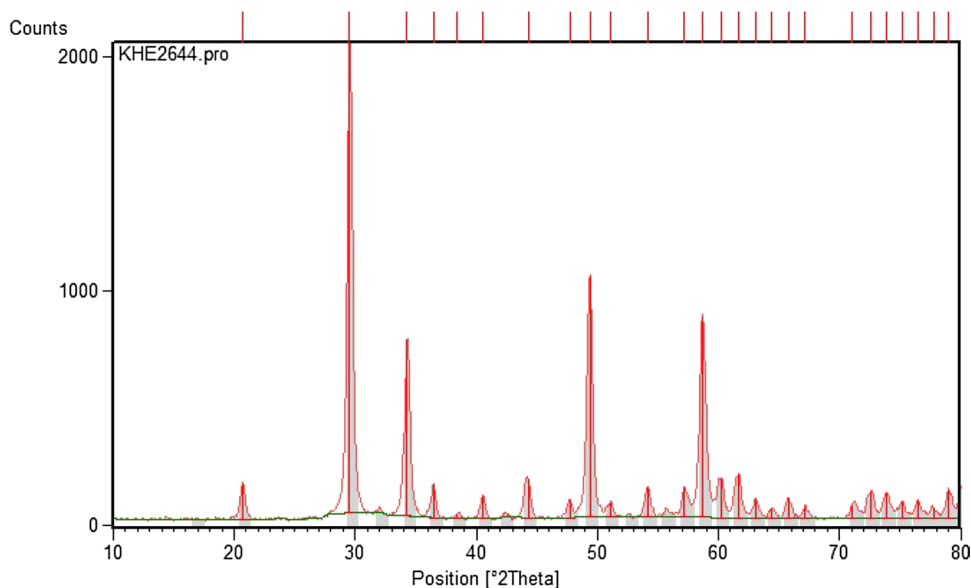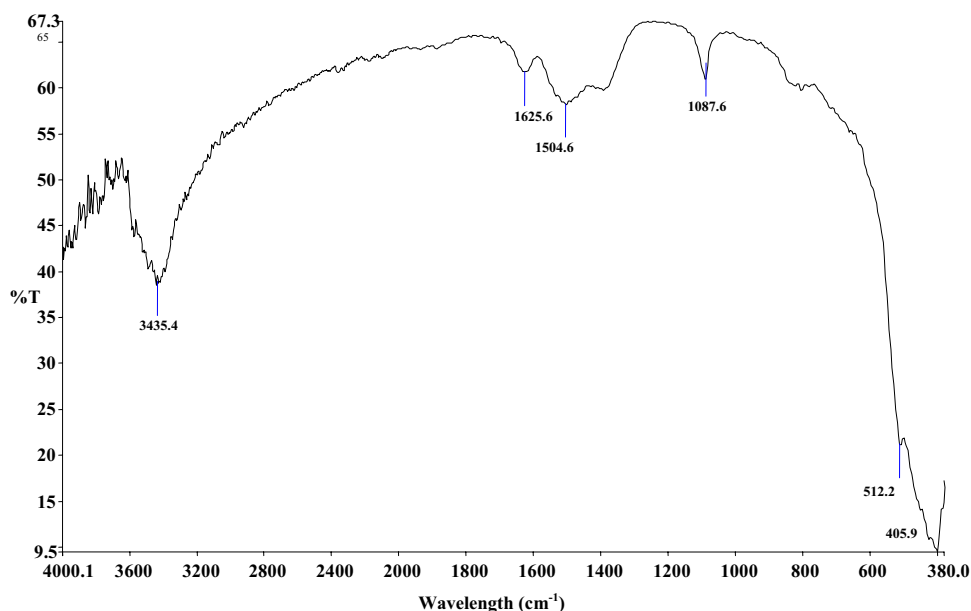**Fig. 10** XRD pattern of the lutetium oxide nanoparticles prepared by thermal decomposition of precursor

Fig. 11 FT-IR spectrum of Lu₂O₃ nanoparticles after calcination of precursor at 350 °C during 4 h

levels cause's slight changes in the outcome. Additionally, results obtained through ANOVA (Table 2) further proved the respective strong and weak relations between the concentrations of the cation and anion solutions on the outcome of the reaction in terms of the particle size.

Figure 2b illustrates the effects of changing in the levels of used flow rate for addition of Lu^{3+} reagent to the reactor (at the three levels of 2.5, 10, and 40 mL/min) on the diameter of lutetium carbonate particles. ANOVA results (Table 2) indicating the significant effect of this parameter on the resulting product. Also, Fig. 2b also illustrates the

effect of the variation in the level of reactor temperature on the size of the produced particles as another studied variable produces a considerable change on the diameter of synthesized nanoparticles proving it to be a significant factor influencing the properties of the product, which is also consistent with the lutetium carbonate particles. The results of ANOVA results summarized in Table 2.

The ANOVA results in Table 2 show that at a confidence level of 90% except for the concentration of carbonate ion, all other parameters (i.e. Lu^{3+} ion concentration, Fy, and reactor temperature) leave considerable effects on
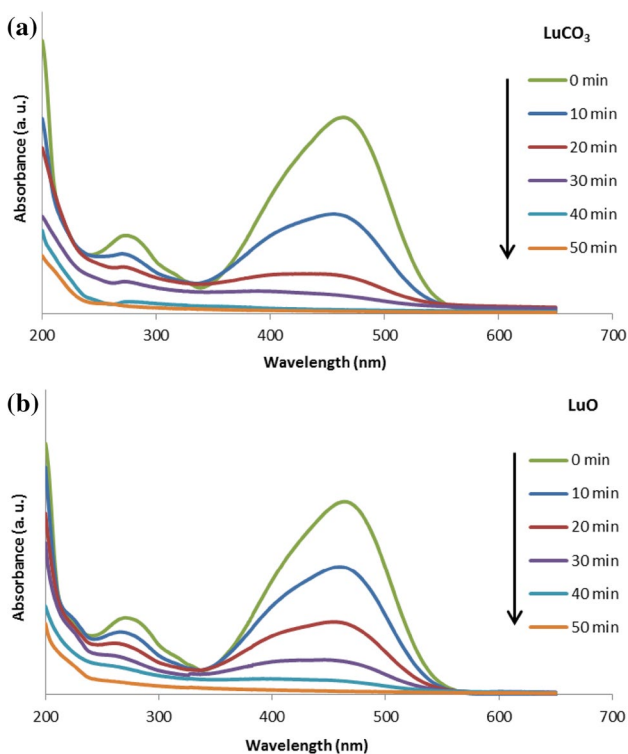
Fig. 12 UV–Vis absorbance spectrum of MO at different time intervals on irradiation using 0.1 g/L, **a** lutetium carbonate (LuCO₃), and **b** lutetium oxide (LuO) nanoparticles as photocatalyst

the properties of the resulting nano–particles, given the fact that the interactions among the variables were not taken into account.

Based on the ANOVA results and the particle size/parameter level profiles in Fig. 2, 0.09 M for the concentration of the lutetium ion solution, 2.5 mL/min for Fy and 0 °C as the reactor temperature can be considered as the optimal parameters for obtaining the best product. Based on the Taguchi experiment design method [49, 50], the optimal outcome (the size of the product particles here) is expressed by:

$$Y_{opt} = \frac{T}{N} + \left(C_x - \frac{T}{N} \right) + \left(F_y - \frac{T}{N} \right) + \left(Tem_z - \frac{T}{N} \right)$$

T being the sum of the average product size in each run, N being the total number of runs, and C_X, F_y, and Tem_z illustrate the optimal Lu^{3+} concentration, flow rate, and temperature, and Y_{opt} is diameter of the optimally prepared product particles. Using the above-mentioned equation the optimal diameter of the produced lutetium carbonate nanoparticles were calculated to be 32.6 ± 4.5 nm.

3.1 Characterization experiments

Once the optimal conditions were determined and the best product was synthesize it was characterized. The result of

the morphology studies by SEM, as presented in Fig. 3a proves the average size of the optimal product to be 35 nm. This was reconfirmed by TEM results (Fig. 3b).

The results of the FT-IR analysis of the optimal product (Fig. 4) revealed absorption bands indicating the presence of various groups. The broad band at 3449.7 cm⁻¹ was attributed to the stretching's and bending of water molecules [44], and the split band at 1519.3 and 1393.4 cm⁻¹ were attributed to the v_3 mode of the carbonate group. The splitting results from the non-equivalent crystallographic locations of the carbonate ions. The bands observed at 1080.1, 850.8, 748.9 and 674.9 cm⁻¹ were also assigned to the stretching modes the anion [9, 44].

UV–Vis spectroscopy was used to evaluate the absorption properties of the product and the results of the analysis on a water dispersion of the sample (Fig. 5) revealed that main absorption to occur in the 240–290 nm window, confirming the small crystal size of the particles, reflecting the strong quantum confinement of the excitonic transition for nanostructures [9].

Thermal stability of samples can be studied by techniques such as DSC, DTA and TG [51]. Thermal evaluations can present data for pre-formulation and development of new compounds [52]. Consequently, thermal analyses were performed to assess the thermal stability of the optimal product. The TG-DTA result illustrated in Fig. 6 represents were obtained for the optimal lutetium carbonate·xH₂O nanoparticles.

Figure 7a, b illustrate the UV–Vis DRS of the nanoparticles and Fig. 8a, b represent the Tauc's plots for the carbonate and oxide nanoparticles, based on which the OBGEs of lutetium carbonate is determined to be around 4 eV and that of lutetium oxide is about 3.7 eV, which correspond to absorption edges of around 310 and 335 nm, respectively.

3.2 Preparation of lutetium oxide nanoparticles

As formerly described, lutetium oxide nanoparticles were prepared by thermally treating the lutetium carbonate precursor at 750 °C for 3 h. The SEM result (Fig. 9) indicates the product to be spherical of about 36 nm in diameter.

The nanoparticles were further evaluated by XRD and FT-IR techniques. The XRD result (Fig. 10) includes diffraction peaks which comply with a cubic Lu_2O_3 phase according to JCPDS 00-012-0728. The XRD spectrum further proved high crystallinty and purity. The FT-IR spectrum (Fig. 11) was found to be in complete agreement with the reports in the literature [9] proving the formation of Lu_2O_3, as reflected by the absorption bands observed at 512.2 and 405.9 cm⁻¹ which correspond to the vibration modes of Lu–O [44].

Fig. 13 Photocatalytic degradation of MO solution under UV irradiation using, **a** lutetium carbonate (LuCO$_3$), and **b** lutetium oxide (LuO) nanoparticles as photocatalyst
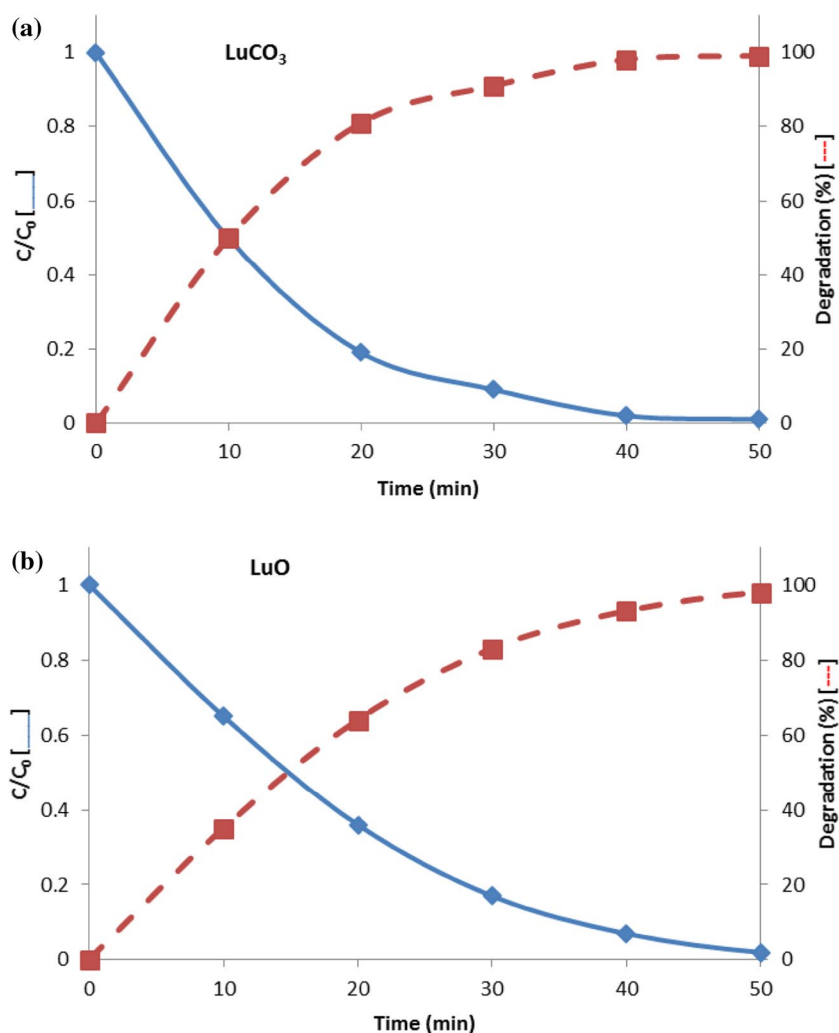
3.3 Evaluation of the photodegradation behavior

The catalytic activities of the lutetium carbonate and lutetium oxide nanoparticles prepared under optimal conditions are illustrated in Fig. 12. Also, Fig. 13 shows the plots of C/C$_0$ and degradation efficiencies against time of illumination, obtained in the presence of the nanoparticles. It can be concluded that the degradation of MO reaches its maxima of about 99 and 98% for the carbonate and oxide salts after 50 min.

On the other hand, Fig. 14 illustrates the $-\ln(C/C_0)$ versus irradiation time plots for both nanoparticles and indicates pseudo first order kinetic behaviors for both nanoparticles. These values together with the first-order reaction rate constants obtained from the slopes of the linear regressions are summarized in Table 3. The data reveal both of carbonate and oxide nanoparticles to offer good efficiencies for eliminating MO and possibly other organic pollutants, yet the rate of degradation is higher in the case of lutetium carbonate.

4 Conclusion

Spherical lutetium carbonate and oxide nanoparticles were prepared through DPR and thermal decomposition of the carbonate salt as the precursor. The parameters influencing the DPR were optimized so as to produce nano-sized products, using the Taguchi robust design. The study proved that synthesis of lutetium carbonate through DPR can be optimized through controlling the reaction parameters with the aim of producing product particles of minimal size. The results of further illustrated that fine spherical lutetium oxide nanoparticles could be prepared through the thermal decomposition of the produced lutetium carbonate nanoparticles as the precursor. The overall method can be considered as a simple, cost-effective method with great potential scale up. The results also showed that the prepared nanoparticles can act as promising photocatalyst for removing MB upto 99% and 98% after 50 min under UV light, respectively.
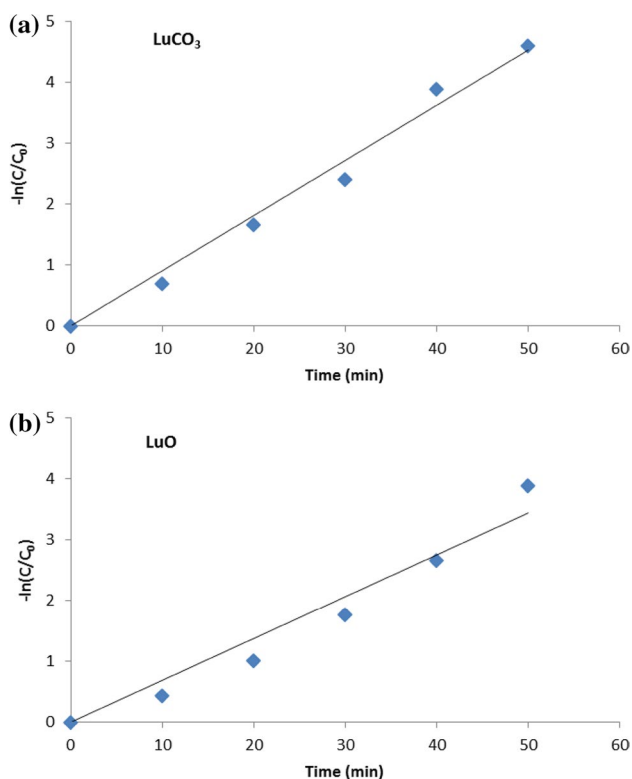
(a)

(b)

Fig. 14 Pseudo first order kinetics of MO degradation for, **a** lutetium carbonate (LuCO$_3$), and **b** lutetium oxide (LuO) nanoparticles

Table 3 Pseudo first order reaction rate constant and conversion efficiency of photocatalysts

	K (min^{-1}) at 50 min	Conversion (%) at 40 min	Conversion (%) at 50 min
Lutetium carbonate	0.0906	98	99
Lutetium oxide	0.0689	93	98

References

1. S.A. Ziarati, A. Badiei, G.M. Ziarani, H. Eskandarloo, Catal. Commun. **95**, 77 (2017)
2. J. Safaei-Ghomi, A. Ziarati, J. Iran. Chem. Soc. **10**, 135 (2013)
3. A. Sobhani-Nasab, M. Maddahfar, S.M. Hosseinpour-Mashkani, J. Mol. Liq. **216**, 1 (2016)
4. M. Mousavi, A. Habibi-Yangjeh, J. Colloid Interface Sci. **465**, 83 (2016)
5. A. Javidan, M. Ramezani, A. Sobhani-Nasab, S.M. Hosseinpour-Mashkani, J. Mater. Sci. Mater. Electron. **26**, 3813 (2015)
6. M. Shekofteh-Gohari, A. Habibi-Yangjeh, J. Colloid Interface Sci. **461**, 144 (2016)
7. S.M. Hosseinpour-Mashkani, A. Sobhani-Nasab, J. Mater. Sci. Mater. Electron. **27**, 7548 (2016)
8. V. Taghvaei, A. Habibi-Yangjeh, M. Behboudnia, J. Iran Chem. Soc. **7**, S175 (2010)
9. M. Rahimi-Nasrabadi, S.M. Pourmortazavi, M.R. Ganjali, P. Novrouzi, F. Faridbod, M.S. Karimi, J. Mater. Sci. Mater. Electron. **28**, 3325 (2017)
10. S.M. Hosseinpour-Mashkani, A. Sobhani-Nasab, J. Mater. Sci. Mater. Electron. **28**, 4345 (2017)
11. I.E. Kolesnikov, D.V. Mamonova, E. Lähderanta, A.V. Kurochkin, M.D. Mikhailov, J. Lumin. **187**, 26 (2017)
12. T. Wiktorczyk, Thin Solid Films **522**, 463 (2012)
13. E. Bonera, G. Scarel, M. Fanciulli, Phys. Rev. Lett. **94**, 027602 (2005)
14. S. Ohmi, H. Takeda, H. Ishiwara, H. Iwai, J. Electrochem. Soc. **151**, G279 (2004)
15. D. Kulesza, P. Bolek, A.J.J. Bos, E. Zych, Coord. Chem. Rev. **325**, 29 (2016)
16. M. Rahimi-Nasrabadi, S.M. Pourmortazavi, M. Aghazadeh, M.R. Ganjali, M.S. Karimi, P. Norouzi, J. Mater. Sci. Mater. Electron. **28**, 9478 (2017)
17. G. Alombert-Goget, Y. Guyot, M. Guzik, G. Boulon, A. Ito, T. Goto, A. Yoshikawa, M. Kikuchi, Opt. Mater. **41**, 3 (2015)
18. J. Wang, Q. Liu, Q.F. Liu, J. Mater. Chem. **15**, 4141 (2005)
19. J. Yang, C.X. Li, Z.W. Quan, C.M. Zhang, P.P. Yang, Y.Y. Li, C.C. Yu, J. Lin, J. Phys. Chem. C **112**, 12777 (2008)
20. G. Jia, Y. Zheng, K. Liu, Y. Song, H. You, H. Zhang, J. Phys. Chem. C **113**, 153 (2009)
21. Y.V. Yermolayeva, A.V. Tolmachev, T.I. Korshikova, R.P. Yavetskiy, M.V. Dobrotvorskaya, N.I. Danylenko, D.S. Sofronov. Nanotechnology **20**, 325601 (2009)
22. J. Yang, C.M. Zhang, C. Peng, C.X. Li, L.L. Wang, R.T. Chai, J. Lin, Chem. Eur. J. **15**, 4649 (2009)
23. M. Esmaili, A. Habibi-Yangjeh, J. Iran, Chem. Soc. **7**, S70 (2010)
24. M. Mousavi, A. Habibi-Yangjeh, M. Abitorabi, J. Colloid Interface Sci. **480**, 218 (2016)
25. M. Rahimi-Nasrabadi, J. Mater. Sci. Mater. Electron. **28**, 2200 (2017)
26. M. Rahimi-Nasrabadi, M. Behpour, A. Sobhani-Nasab, M. Rangraz Jeddy, J. Mater. Sci. Mater. Electron. **27**, 11691 (2016)
27. M. Rahimi-Nasrabadi, F. Ahmadi, M. Eghbali-Arani, J. Mater. Sci. Mater. Electron. **27**, 11873 (2016)
28. A. Sobhani-Nasab, S.M. Hosseinpour-Mashkani, M. Salavati-Niasari, S. Bagheri, J. Cluster Sci. **26**, 1305 (2015)
29. F. Ahmadi, M. Rahimi-Nasrabadi, A. Fosooni, M.H. Daneshmand, J. Mater. Sci. Mater. Electron. **27**, 9514 (2016)
30. A. Sobhani-Nasab, M. Behpour, J. Mater. Sci. Mater. Electron. **27**, 11946 (2016)
31. M. Rahimi-Nasrabadi, J. Mater. Sci. Mater. Electron. **28**, 6373 (2017)
32. H. Rezaei-Vahidian, A.R. Zarei, A.R. Soleymani, J. Hazard. Mater. **325**, 310 (2017)
33. S. Ramandi, M.H. Entezari, N. Ghows, Ultrason. Sonochem. **38**, 234 (2017)
34. J. Yao, H. Chen, F. Jiang, Z. Jiao, M. Jin, J. Colloid Interface Sci. **490**, 154 (2017)
35. A. Ebrahimian Pirbazari, Procedia Mater. Sci. **11**, 622 (2015)
36. M. Sarkarat, S. Komarneni, Z. Rezvani, X. Wu, S. Yin, T. Sato, Z. Yan, Appl. Clay Sci. **80–81**, 390 (2013)
37. M. Ramezani, A. Sobhani-Nasab, S.M. Hosseinpour-Mashkani, J. Mater. Sci. Mater. Electron. **26**, 4848 (2015)
38. S.M. Pourmortazavi, M. Rahimi-Nasrabadi, Y. Fazli, M. Mohammad-Zadeh, Int. J. Refract. Met. Hard Mater. **51**, 29 (2015)
39. M. Rahimi-Nasrabadi, S.M. Pourmortazavi, M. Khalilian-Shalamzari, J. Mol. Struct. **1083**, 229 (2015)

40. S.M. Pourmortazavi, S.S. Hajimirsadeghi, M. Rahimi-Nasrabadi, Mater. Sci. Semicond. Process. **16**, 131 (2013)

41. M. Rahimi-Nasrabadi, S.M. Pourmortazavi, M. Khalilian-Shalamzari, S.S. Hajimirsadeghi, M.M. Zahedi, Open Chem. **11**, 1393 (2013)

42. M. Rahimi-Nasrabadi, S.M. Pourmortazavi, M.R. Ganjali, A.R. Banan, F. Ahmadi, J. Mol. Struct. **1074**, 85 (2014)

43. M. Rahimi-Nasrabadi, S.M. Pourmortazavi, M. Aghazadeh, M.R. Ganjali, M.S. Karimi, P. Norouzi, J. Mater. Sci. Mater. Electron. **28**, 7600 (2017)

44. M. Rahimi-Nasrabadi, S.M. Pourmortazavi, M. Aghazadeh, M.R. Ganjali, M.S. Karimi, P. Novrouzi, J. Mater. Sci. Mater. Electron. **28**, 5574 (2017)

45. M. Rahimi-Nasrabadi, S.M. Pourmortazavi, M.R. Ganjali, P. Norouzi, F. Faridbod, M.S. Karimi, J. Mater. Sci. Mater. Electron. **27**, 12860 (2016)

46. A. Sobhani-Nasab, M. Rangraz-Jeddy, A. Avanes, M. Salavati-Niasari, J. Mater. Sci. Mater. Electron. **26**, 9552 (2015)

47. M. Rahimi-Nasrabadi, H.R. Naderi, M.S. Karimi, F. Ahmadi, S.M. Pourmortazavi, J. Mater. Sci. Mater. Electron. **28**, 1877 (2017)

48. M. Rahimi-Nasrabadi, S.M. Pourmortazavi, M.S. Karimi, M. Aghazadeh, M.R. Ganjali, P. Norouzi, J. Mater. Sci. Mater. Electron. **28**, 6399 (2017)

49. K. Adib, M. Rahimi-Nasrabadi, Z. Rezvani, S.M. Pourmortazavi, F. Ahmadi, H.R. Naderi, M.R. Ganjali, J. Mater. Sci. Mater. Electron. **27**, 4541 (2016)

50. M. Rahimi-Nasrabadi, S.M. Pourmortazavi, M.R. Ganjali, P. Norouzi, J. Mater. Sci. Mater. Electron. **28**, 9724 (2017)

51. S.M. Pourmortazavi, M. Rahimi-Nasrabadi, I. Kohsari, S.S. Hajimirsadeghi, J. Therm. Anal. Calorim. **110**, 857 (2012)

52. S.S. Hajimirsadeghi, M.B. Teimouri, M. Rahimi-Nasrabadi, S. Dehghanpour. J. Therm. Anal. Calorim. **98**, 463 (2009)